

# Prediction of Aluminum Combustion Efficiency in Solid Propellant Rocket Motors

Richard S. Larson\*

*Sandia National Laboratories, Livermore, California*

Aluminum combustion efficiencies in solid propellant rocket motors are calculated by means of an improved theoretical model for the physical and chemical processes involved. In particular, more complete allowance is made for the fact that the gas-phase concentration of oxidizing species in the rocket chamber varies from point to point as a result of depletion by the aluminum combustion reaction. Analyses are carried out for both one-dimensional and two-dimensional gas flowfields and both with and without consideration of particle velocity lags. Numerical calculations indicate that the neglect of variations in the oxidizer concentration  $\alpha$  leads to significant errors when the combustion efficiency is substantially less than unity. These errors can be effectively eliminated, with little additional effort, by accounting for the variations in  $\alpha$  under the assumption that particles of different sizes may be treated independently and that oxidizer depletion is not seriously affected by velocity lags.

## Introduction

COMPOSITE propellants used in modern solid rocket motors generally contain powdered aluminum in addition to an ammonium perchlorate (AP) oxidizer and a polymeric binder. While the use of this metallic fuel can have the beneficial effect of suppressing combustion instabilities, the most obvious reason for its introduction is the resulting increase in the specific impulse of the rocket. However, this improvement in performance is invariably accompanied by a decrease in the specific impulse efficiency, i.e., the ratio of the observed impulse to its theoretical maximum value. Most of this decrease can be attributed to the thermal and velocity lags of the particulate (aluminum oxide) products as they pass through the nozzle, but incomplete combustion of the aluminum in the rocket chamber may also be a factor. Thus, an analysis of Al combustion efficiency is important to the accurate prediction of rocket performance, and it may also be useful in understanding the related problems of  $\text{Al}_2\text{O}_3$  formation, slag deposition, and plume development.

In order to calculate the aluminum combustion efficiency of a motor, it is necessary to have a reasonably detailed idea of the way in which aluminum particles burn in the chamber. This is, by all accounts, an exceedingly complex process, but a description of the most commonly observed chain of events can be given.<sup>1</sup> The key feature underlying the whole scenario is that, since Al particles are not easily ignited, they do not burn in the region where the AP/binder combustion takes place. Thus, the first step is the accumulation of aluminum at the burning propellant surface as the latter recedes. Being protected by a solid oxide shell, a particle does not ignite even when the Al melting point is reached; instead, neighboring particles tend to adhere to one another through sintering of their respective shells. Eventually, upon melting (at 2300 K) or fracture of the oxide covering, the aluminum in an agglomerate ignites and coalesces into a spherical drop. This disrupts the surface tension forces holding the agglomerate on the surface, so the droplet detaches, enters the chamber cavity, and burns in the AP/binder combustion products with a gas-phase diffusion flame. Finally, the condensed-

phase  $\text{Al}_2\text{O}_3$  product is formed by nucleation of gaseous suboxides and by condensation and/or heterogeneous reaction on the surface of the resulting smoke particles and the burning aluminum droplet.

Only a few attempts have been made to predict the aluminum combustion efficiency from an analysis of the underlying physical and chemical processes. Perhaps the most widely used results are those obtained by Hermesen<sup>2</sup> for use in the Air Force's Solid Propellant Performance (SPP) computer code. These apply specifically to a cylindrical internally burning propellant grain and are based on the following assumptions:

- 1) The combustion of the propellant is a quasi-steady state process.
- 2) The AP/binder reactions are complete at or near the propellant surface (before the Al combustion begins).
- 3) The gas flowfield in the chamber is unaffected by the presence of the particulate phase.
- 4) The physical properties of the gas phase are constant.
- 5) The Al particle combustion is described by the empirical burning-rate law

$$dD/dt = -kD^{-0.8}\alpha^{0.9} \quad (1)$$

where  $k$  is the reaction rate constant,  $D$  the particle diameter, and  $\alpha$  the sum of the gas-phase mole fractions of the oxidizing species (oxidizers for short—not to be confused with the AP in the original propellant).

6) A single constant (average) value of  $\alpha$  can be used. With the aid of an assumed gas flowfield, the burning-rate law and the equations of motion for a given particle are integrated from the propellant surface to the exit plane of the chamber in order to determine the fractional combustion. Averaging over a representative set of initial positions then gives the combustion efficiency  $E$  for particles of the given initial size. The overall value of  $E$  can be found by integrating the results over the actual Al agglomerate size distribution (which may differ greatly from the Al size distribution in the original propellant and which must generally be obtained from experimental measurements).

A similar but more elaborate analysis has been carried out by King<sup>3,4</sup> in order to provide an improved predictive capability, particularly for nozzleless motors. In its treatment of particle combustion within the chamber, this work goes beyond that of Hermesen by accounting, at least approximately, for 1) the effects of compressibility on the gas

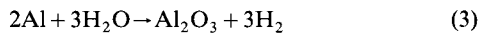
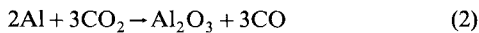
Received Nov. 14, 1985; revision received May 12, 1986. Copyright © American Institute of Aeronautics and Astronautics, Inc., 1986. All rights reserved.

\*Member of Technical Staff, Thermal and Fluid Mechanics Division.

flowfield, 2) enhancement of the burning rate by particle slip, and 3) depletion of oxidizer along a particle trajectory. King acknowledges that the first two of these are not important for ordinary nozzled motors, with which the present work is concerned. Attention will therefore focus here on the way in which the variation in  $\alpha$  is calculated.

King's analysis is based on the concept of a gas-particle pocket that remains isolated from all other such pockets and thus retains its identity as it moves from the propellant surface to the exit plane of the chamber. Unfortunately, this idea is inconsistent with the existence of particle velocity lags, which cause the gas and particles to move along different paths. Furthermore, this approach ignores the fact that, even in the zero-lag case, the concentration of oxidizer at any location is actually affected by particles across the whole spectrum of sizes. Still, it is possible that this approximation (or even Hermesen's assumption of constant  $\alpha$ ) gives results that are entirely adequate for practical purposes. The primary goal of the present work is to assess the validity of the two approaches.

Clearly, in order to develop a rigorous analysis of the way in which the concentration of oxidizer varies within the chamber, one must specify explicitly the chemical reaction(s) involved. Now, an examination of the combustion products of a typical nonaluminized propellant<sup>5</sup> shows that the only substances capable of oxidizing Al to  $\text{Al}_2\text{O}_3$ , which are present in significant quantities, are  $\text{CO}_2$  and  $\text{H}_2\text{O}$ . (At the higher temperatures characteristic of aluminized propellant combustion, it is possible that OH is also important, but the rate of its reaction with Al is not well documented.) Consequently, it will be assumed that the reactions of interest are



The fact that the stoichiometric coefficients are the same in each case, together with the fact that the particle burning rate depends only on a sum of oxidizer concentrations,<sup>6</sup> means that  $\text{CO}_2$  and  $\text{H}_2\text{O}$  can be treated as a single species in the analysis. As will be seen, this simplifies the mathematics considerably.

A comment should be made here concerning the way in which the particle burning rate depends on the particle diameter. Equation (1) implies that the total burning time varies as  $D^{1.8}$  (for fixed  $\alpha$ ); while there is certainly some experimental evidence to support this,<sup>7</sup> other measurements are consistent with a  $D^{1.5}$  law,<sup>6</sup> which is used by King.<sup>3</sup> Furthermore, theoretical investigations have suggested values of the exponent that range from 1.35 to 1.90.<sup>8</sup> (On the other hand, there appears to be no controversy with regard to the dependence of  $dD/dt$  on  $\alpha$ .) Thus, it seems best to leave the exponent (call it  $p$ ) unspecified for the moment, whereupon Eq. (1) becomes

$$dD/dt = -kD^{1-p}\alpha^{0.9} \quad (4)$$

In what follows, the Al combustion efficiency is first calculated for a model that uses a one-dimensional gas flowfield and neglects particle velocity lags. The adequacy of the one-dimensional approximation is then tested by repeating the analysis for the more realistic, but more complicated, case of a two-dimensional flowfield. The results are compared with those obtained from two simplified two-dimensional models, one of which assumes (along with King) that the variation in  $\alpha$  along a particle trajectory can be determined independently for particles of different sizes (so that the initial size distribution need not be known a priori), and the other of which ignores the variation in  $\alpha$  entirely (as in Hermesen's work). On the basis of this comparison, three simplified models that take particle velocity lags into account are formulated and evaluated.

## Analysis and Numerical Results

The first step in computing the Al combustion efficiency is to write down an expression for the molar rate at which aluminum enters the flowfield from the propellant surface between the closed end of the chamber ( $x=0$ ) and an arbitrary axial position  $x$ :

$$\begin{aligned} \dot{m}_0 &= \int_0^x \int_0^\infty \frac{\pi}{6} D_0^3 \frac{\rho_{\text{Al}}}{M_{\text{Al}}} F(D_0) dD_0 \cdot 2\pi R \dot{n}_0 dx_0 \\ &= \frac{\pi^2 \rho_{\text{Al}} R \dot{n}_0}{3M_{\text{Al}}} \langle D_0^3 \rangle x \end{aligned} \quad (5)$$

Here  $\rho_{\text{Al}}$  and  $M_{\text{Al}}$  are the liquid-phase density and molecular weight, respectively, of aluminum,  $R$  the chamber radius,  $D_0$  the initial diameter of a particle (agglomerate),  $x_0$  the position at which it leaves the surface,  $\dot{n}_0$  the total number of particles entering the gas phase per unit area per unit time, and  $F(D_0)$  the normalized agglomerate size distribution function (i.e.,  $F(D_0)dD_0$  is the fraction of particles having initial diameters between  $D_0$  and  $D_0 + dD_0$ ); the angle brackets denote an average over this distribution. The molar flow rate of unburned aluminum past position  $x$  can be obtained simply by replacing  $D_0^3$  in the integral with  $D^3$ , where  $D$  is understood to be the diameter at  $x$  of a particle that had diameter  $D_0$  at  $x_0$ :

$$\dot{m} = \frac{\pi^2 \rho_{\text{Al}} R \dot{n}_0}{3M_{\text{Al}}} \int_0^x \int_0^\infty [D(D_0, x_0, x)]^3 F(D_0) dD_0 dx_0 \quad (6)$$

The overall combustion efficiency between 0 and  $x$  is then given by

$$\bar{E} = 1 - \frac{\dot{m}}{\dot{m}_0} \quad (7)$$

$$= 1 - \frac{1}{\langle D_0^3 \rangle x} \int_0^x \int_0^\infty D^3 F(D_0) dD_0 dx_0 \quad (8)$$

$$= \frac{1}{\langle D_0^3 \rangle} \int_0^\infty D_0^3 F(D_0) \left( 1 - \frac{1}{D_0^3 x} \int_0^x D^3 dx_0 \right) dD_0 \quad (9)$$

$$\equiv \frac{1}{\langle D_0^3 \rangle} \int_0^\infty D_0^3 F(D_0) E(D_0, x) dD_0 \quad (10)$$

which is clearly just the volume average of the efficiencies for individual values of  $D_0$ .

The computation of  $\bar{E}$  is thus reduced, in essence, to a determination of the way in which  $D$  depends on  $D_0$ ,  $x_0$ , and  $x$ . The required relationship can be obtained for any one of a number of different models, each of which will now be considered in turn.

### One-Dimensional Flowfield with Particle Velocity Lags Neglected

If the axial particle (and gas) velocity is denoted by  $u = dx/dt$ , then Eq. (4) becomes

$$u \frac{\partial D}{\partial x} = -kD^{1-p}\alpha^{0.9} \quad (11)$$

where the partial derivative notation has been used in order to emphasize that  $D_0$  and  $x_0$  are being held constant. Upon integration, this gives

$$D = \left( D_0^p - pk \int_{x_0}^x \frac{\alpha^{0.9}}{u} dx' \right)^{1/p} \quad (12)$$

provided that the quantity in parentheses is nonnegative; otherwise  $D$  is simply equal to zero. Now,  $u$  can be found by balancing the molar flow rate of gas at position  $x$  with the rate at which gas is released at the surface due to propellant combustion between 0 and  $x$ :

$$\pi R^2 u c = 2\pi R x \dot{r}_s N \quad (13)$$

so that

$$u = (2\dot{r}_s N / Rc) x \quad (14)$$

Here  $c$  is the molar density of the gas phase (assumed constant),  $\dot{r}_s$  the linear rate at which the propellant surface recedes, and  $N$  the number of moles of gas produced per unit volume of propellant burned. The oxidizer mole fraction  $\alpha$  can be obtained in a like manner, except that an additional term accounting for consumption of oxidizer in the Al combustion reaction must be included. (Such a term is absent from Eq. (13) because Eqs. (2) and (3) show no net change in the total number of moles in the gas phase.) Thus,

$$\pi R^2 u c \alpha = 2\pi R x \dot{r}_s N \alpha_0 - (3/2)(\dot{m}_0 - \dot{m}) \quad (15)$$

where  $\alpha_0$  is the value of  $\alpha$  in the propellant combustion products and the stoichiometric ratio 3/2 is taken from Eqs. (2) and (3). Substituting for  $u$  and solving (at least formally) for  $\alpha$  gives

$$\alpha = \alpha_0 - \frac{3(\dot{m}_0 - \dot{m})}{4\pi R x \dot{r}_s N} \quad (16)$$

It can now be shown that  $\alpha$  is, in fact, a constant in this model (although it is not equal to  $\alpha_0$ —this situation results from the assumption of perfect radial mixing). For, if this is true, then Eq. (12) becomes [upon substitution of Eq. (14)]

$$D = \left( D_0^p - \frac{pk\alpha^{0.9} Rc}{2\dot{r}_s N} \ln \frac{x}{x_0} \right)^{1/p} \quad (17)$$

and insertion into Eq. (6) gives

$$\dot{m} = \frac{\pi^2 \rho_{Al} R \dot{r}_0 x}{3M_{Al}} \int_0^\infty F(D_0) \times \int_{\xi_{\min}}^1 \left( D_0^p + \frac{pk\alpha^{0.9} Rc}{2\dot{r}_s N} \ln \xi \right)^{3/p} d\xi dD_0 \quad (18)$$

where  $\xi = x_0/x$  and

$$\xi_{\min} = \exp \left( -\frac{2D_0^p \dot{r}_s N}{pk\alpha^{0.9} Rc} \right) \quad (19)$$

Since, according to Eqs. (5) and (18),  $\dot{m}_0$  and  $\dot{m}$  are both proportional to  $x$ , Eq. (16) shows that  $\alpha$  is independent of  $x$ , as asserted. Significantly, it follows from Eq. (7) that the same is true of  $\bar{E}$ .

If Eq. (18) is now rewritten in terms of the new variable

$$z = \frac{-pk\alpha^{0.9} Rc}{2\dot{r}_s ND_0^p} \ln \xi \quad (20)$$

and the result is substituted, along with Eq. (5), into Eq. (7), then the overall combustion efficiency is found to be

$$\bar{E} = 1 - \frac{1}{\langle D_0^3 \rangle} \int_0^\infty D_0^3 F(D_0) \times \int_0^1 (1-z)^{3/p} \exp \left[ -\theta \left( \frac{\alpha_0}{\alpha} \right)^{0.9} z \right] \theta \left( \frac{\alpha_0}{\alpha} \right)^{0.9} dz dD_0 \quad (21)$$

where

$$\theta = \frac{2\dot{r}_s ND_0^p}{pk\alpha_0^{0.9} Rc} \quad (22)$$

As is easily verified, the parameter  $\theta$  is the ratio of the burning time of a particle of initial diameter  $D_0$  in a gas for which  $\alpha \equiv \alpha_0$  to the mean residence time in the chamber; as such, it is expected to be of central importance in determining  $E(D_0)$ . Equation (21) can be simplified somewhat via an integration by parts:

$$\bar{E} = \frac{3}{p \langle D_0^3 \rangle} \int_0^\infty D_0^3 F(D_0) \times \int_0^1 (1-z)^{3/p-1} \exp \left[ -\theta \left( \frac{\alpha_0}{\alpha} \right)^{0.9} z \right] dz dD_0 \quad (23)$$

Finally,  $\alpha$  can be expressed in terms of  $\bar{E}$  by combining Eqs. (5), (7), and (16):

$$\alpha = \alpha_0 - \frac{\pi \langle D_0^3 \rangle \dot{r}_0 \rho_{Al}}{4\dot{r}_s N M_{Al}} \bar{E} \quad (24)$$

Equation (23) now becomes

$$\bar{E} = \frac{3}{p \langle D_0^3 \rangle} \int_0^\infty D_0^3 F(D_0) \times \int_0^1 (1-z)^{3/p-1} \exp \left[ -\theta (1-\phi \bar{E})^{-0.9} z \right] dz dD_0 \quad (25)$$

where

$$\phi = \frac{\pi \langle D_0^3 \rangle \dot{r}_0 \rho_{Al}}{4\dot{r}_s N M_{Al} \alpha_0} \quad (26)$$

is the ratio of the molar fluxes of aluminum and oxidizer away from the propellant surface, corrected by the stoichiometric factor 3/2. Equation (25) thus gives  $\bar{E}$  implicitly in terms of the relevant parameters. Comparison with Eq. (10) shows that

$$E(D_0) = \frac{3}{p} \int_0^1 (1-z)^{3/p-1} \exp \left[ -\theta (1-\phi \bar{E})^{-0.9} z \right] dz \quad (27)$$

and the presence of  $\bar{E}$  on the right-hand side demonstrates clearly that combustion efficiencies for particles of different initial diameters cannot, in general, be calculated independently.

In a later section, Eq. (25) will be compared numerically with the results of the several two-dimensional models now to be discussed.

#### Two-Dimensional Flowfield with Particle Velocity Lags Neglected

The flowfield to be used here is one proposed originally by Culick,<sup>9</sup> verified experimentally by Dunlap et al.,<sup>10</sup> and later adopted for use by Hermesen.<sup>2</sup> In terms of the cylindrical coordinates  $x$  and  $r$ , the corresponding velocity components  $u$  and  $v$  are given by

$$u = \frac{\pi \dot{r}_s N x}{Rc} \cos \left[ \frac{\pi}{2} \left( \frac{r}{R} \right)^2 \right] \quad (28)$$

$$v = -\frac{\dot{r}_s N R}{cr} \sin \left[ \frac{\pi}{2} \left( \frac{r}{R} \right)^2 \right] \quad (29)$$

The way in which  $x$  and  $r$  are related along a particle trajectory can be found by writing

$$\frac{dx}{dr} = \frac{u}{v} = -\frac{\pi x r}{R^2} \cot \left[ \frac{\pi}{2} \left( \frac{r}{R} \right)^2 \right] \quad (30)$$

which, on integration, becomes

$$x = x_0 \csc \left[ \frac{\pi}{2} \left( \frac{r}{R} \right)^2 \right] \quad (31)$$

This can be used to eliminate  $r$  in favor of  $x_0$  in Eq. (28):

$$u = \frac{\pi \dot{r}_s N}{Rc} (x^2 - x_0^2)^{1/2} \quad (32)$$

Fortunately, this result is only slightly more complicated than the one-dimensional version, Eq. (14).

The next step is to evaluate the consumption rate of oxidizer at any point in the chamber, and this depends on the number density  $n$  of aluminum particles at that point. Assuming that there is no significant agglomeration or fragmentation of particles in the chamber cavity,  $n$  is governed by the conservation equation

$$0 = \nabla \cdot (n\mathbf{u}) = n \nabla \cdot \mathbf{u} + \mathbf{u} \cdot \nabla n = \mathbf{u} \cdot \nabla n \quad (33)$$

[ $\mathbf{u} \equiv (u, v)$  being the velocity vector], where the last equality follows from the fact that  $\mathbf{u}$  satisfies the continuity equation for incompressible flow. (It should be mentioned that, for present purposes, a particle is still considered to exist even after its size has been reduced to zero.) It follows that  $n$  is constant along the gas (or particle) streamlines; however, since all streamlines emanate from the propellant surface, every point of which is assumed to have the same properties,  $n$  must be uniform throughout the chamber. Its value can be determined from the flux balance

$$\dot{n}_0 = -vn|_{r=R} = (\dot{r}_s N/c)n \quad (34)$$

so that

$$n = c\dot{n}_0/\dot{r}_s N \quad (35)$$

In terms of  $n$ , the molar consumption rate of aluminum per unit volume in the chamber is given by

$$\begin{aligned} -n \frac{d}{dt} \left[ \int_0^\infty \frac{\pi}{6} D^3 \frac{\rho_{Al}}{M_{Al}} F(D_0) dD_0 \right] \\ = -\frac{n\pi\rho_{Al}}{2M_{Al}} \int_0^\infty D^2 \frac{dD}{dt} F(D_0) dD_0 \end{aligned} \quad (36)$$

With the aid of Eq. (4), the right-hand side becomes

$$\frac{\pi n k \rho_{Al}}{2M_{Al}} \alpha^{0.9} \int_{D_0^*}^\infty D^{3-p} F(D_0) dD_0$$

where  $D_0^*$  is the smallest value of  $D_0$  for which  $D$  is nonzero at the point in question. This is now multiplied by the stoichiometric ratio 3/2 and set equal to  $-c(d\alpha/dt)$  to give

$$\frac{d\alpha}{dt} = -\frac{3\pi n k \rho_{Al}}{4M_{Al}c} \alpha^{0.9} \int_{D_0^*}^\infty D^{3-p} F(D_0) dD_0 \quad (37)$$

This, in turn, can be combined with Eq. (4) in order to eliminate the pseudovaryable  $t$ , thus yielding a differential relationship between  $D$  and  $\alpha$ :

$$\frac{dD}{d\alpha} = \frac{4M_{Al}cD^{1-p}}{3\pi n \rho_{Al}} \left[ \int_{D_0^*(\alpha)}^\infty D^{3-p} F(D_0) dD_0 \right]^{-1} \quad (38)$$

Unfortunately, it does not appear that a general analytical solution to Eq. (38) can be found. However, there are (at least) two special cases for which the equation can be solved without great difficulty. In one of these,  $F(D_0)$  is taken to be a delta function, i.e., all of the particles are assumed to have the same initial diameter. Equation (38) then reduces to

$$\frac{dD}{d\alpha} = \frac{4M_{Al}c}{3\pi n \rho_{Al} D^2} \quad (39)$$

which, when integrated subject to the condition that  $D=D_0$  when  $\alpha=\alpha_0$ , gives

$$\alpha = \alpha_0 + \frac{\pi n \rho_{Al}}{4M_{Al}c} (D^3 - D_0^3) \quad (40)$$

Substitution of Eqs. (32) and (40) into Eq. (11), which is still valid here, then yields

$$\frac{\partial D}{\partial x} = \frac{-kRcD^{1-p}}{\pi \dot{r}_s N (x^2 - x_0^2)^{1/2}} \left[ \alpha_0 + \frac{\pi n \rho_{Al}}{4M_{Al}c} (D^3 - D_0^3) \right]^{0.9} \quad (41)$$

the integrated form of which is

$$\begin{aligned} \int_D^{D_0} \left[ \alpha_0 + \frac{\pi n \rho_{Al}}{4M_{Al}c} (y^3 - D_0^3) \right]^{-0.9} y^{p-1} dy \\ = \frac{kRc}{\pi \dot{r}_s N} \ln \frac{1 + (1 - \xi^2)^{1/2}}{\xi} \end{aligned} \quad (42)$$

where, as before,  $\xi \equiv x_0/x$ . In principle, Eq. (42) can be solved by trial and error to find  $D$  as a function of  $\xi$ , and the result can be used to compute the combustion efficiency via

$$E = 1 - \frac{1}{D_0^3} \int_{\xi_{\min}}^1 D^3 d\xi \quad (43)$$

[Here  $\xi_{\min}$  is the value of  $\xi$  for which Eq. (42) gives  $D=0$ ; the existence of such a value is guaranteed if the equivalence ratio  $\phi$  defined in Eq. (26) is less than or equal to unity, which is always the case in practice.] However, this is a cumbersome procedure; a more efficient algorithm can be developed by differentiating Eq. (42) with respect to  $D$  to give

$$\frac{d\xi}{dD} = \frac{\pi \dot{r}_s N}{kRc} \xi (1 - \xi^2)^{1/2} D^{p-1} \left[ \alpha_0 + \frac{\pi n \rho_{Al}}{4M_{Al}c} (D^3 - D_0^3) \right]^{-0.9} \quad (44)$$

and integrating by parts in Eq. (43), using the fact that  $D=D_0$  when  $\xi=1$ :

$$E = \frac{3}{D_0^3} \int_0^{D_0} \xi D^2 dD \quad (45)$$

Finally, it is convenient to introduce the new variables  $\zeta = 1 - (D/D_0)^p$  and  $\omega = \cos^{-1}\zeta$  in order to render Eqs. (44) and (45) dimensionless and to remove troublesome singularities:

$$E = \frac{3}{p} \int_0^1 (1-\zeta)^{3/p-1} \cos\omega d\zeta \quad (46)$$

where

$$\frac{d\omega}{d\zeta} = \frac{\pi\theta}{2} \cos\omega \{1 + \phi[(1-\zeta)^{3/p} - 1]\}^{-0.9} \quad (47)$$

$\theta$  and  $\phi$  being defined exactly as before. [The striking formal similarity between Eqs. (46) and (27) may be noted.] Thus, all that is necessary is to solve Eq. (47) numerically, using the condition  $\omega(0)=0$ , and then to insert the results into Eq. (46). Just as in the one-dimensional case,  $E$  is independent of  $x$  (and thus of the chamber length), being a function only of the dimensionless parameters  $p$ ,  $\theta$ , and  $\phi$ .

It turns out that Eq. (38) can be solved semianalytically even for arbitrary  $F(D_0)$  if  $p$  has the value  $3/2$ . By fortunate coincidence, this is precisely the value recommended by Pokhil et al.<sup>6</sup> for combustion of aluminum with  $\text{CO}_2$  and  $\text{H}_2\text{O}$  as oxidizers. With this choice, then, Eq. (38) becomes

$$\frac{d}{d\alpha}(D^{3/2}) = \frac{2M_{\text{Al}}c}{\pi n\rho_{\text{Al}}} \left[ \int_{D_0^*(\alpha)}^{\infty} D^{3/2} F(D_0) dD_0 \right]^{-1} \quad (48)$$

This can be converted to an ordinary differential equation by evaluating the integral in terms of  $D_0^*$  and  $F$  alone, eliminating the unknown function  $D_0^*(\alpha)$ , and then differentiating with respect to  $\alpha$ . The details are given in the Appendix, and the result, expressed in terms of the dimensionless quantities  $\zeta = 1 - (D/D_0)^{3/2}$  and  $a = 1 - \alpha/\alpha_0$ , is

$$\begin{aligned} \frac{d^3\zeta}{da^3} &= 3 \left( \frac{d\zeta}{da} \right)^{-1} \left( \frac{d^2\zeta}{da^2} \right)^2 \\ &\quad - \frac{4}{3} \phi \beta \left( \frac{\theta}{\langle\theta\rangle} \right)^2 D_0 F(D_0 \zeta^{2/3}) \zeta^{-1/3} \left( \frac{d\zeta}{da} \right)^4 \end{aligned} \quad (49)$$

[As before, the angle brackets indicate averaging over  $F(D_0)$ .] The parameter  $\beta$  appearing here is defined by

$$\beta \equiv \frac{\langle D_0^{3/2} \rangle^2}{\langle D_0^3 \rangle} \leq 1 \quad (50)$$

and is a measure of the dispersion in the distribution  $F(D_0)$ . The initial conditions to be used in solving Eq. (49) are that  $\zeta=0$ ,  $d\zeta/da = \langle\theta\rangle/2\phi\beta\theta$ , and  $d^2\zeta/da^2 = \langle\theta\rangle/(2\phi\beta)^2\theta$  at  $a=0$ .

The solution thus obtained takes the place of Eq. (40), and the analysis can then be carried out just as before to give

$$E(D_0) = 2 \int_0^1 (1-\zeta) \cos\omega d\zeta \quad (51)$$

where

$$\frac{d\omega}{d\zeta} = \frac{\pi\theta}{2} \cos\omega (1-a)^{-0.9} \quad (52)$$

However, since Eq. (49) gives  $\zeta$  as a function of  $a$ , rather than vice versa, it is more convenient to write all the equations using  $a$  as the independent variable:

$$E(D_0) = 2 \int_0^{a_{\text{max}}} (1-\zeta) \cos\omega \frac{d\zeta}{da} da \quad (53)$$

$$\frac{d\omega}{da} = \frac{\pi\theta}{2} \cos\omega (1-a)^{-0.9} \frac{d\zeta}{da} \quad (54)$$

where  $a_{\text{max}}$  is the value of  $a$  at which  $\zeta=1$ .

It is of interest to compare the foregoing results with those obtained by assuming a constant value of  $\alpha$ , as done by Hermesen.<sup>2</sup> The above analysis indicates that, in the computation of  $E(D_0)$ , the distribution function  $F(D_0)$  affects only the determination of a relationship between  $\alpha$  and  $D$ , and it is therefore irrelevant if the variation in  $\alpha$  is ignored. Consequently, even for arbitrary  $F(D_0)$ ,  $E(D_0)$  is given by Eq. (46), but Eq. (47) is modified to read

$$\frac{d\omega}{d\zeta} = \frac{\pi\theta}{2} \cos\omega \left( \frac{\alpha_0}{\alpha} \right)^{0.9} \quad (55)$$

This, however, can be solved analytically:

$$\zeta = \frac{2}{\pi\theta} \left( \frac{\alpha}{\alpha_0} \right)^{0.9} \ln(\sec\omega + \tan\omega) \quad (56)$$

Substitution into Eq. (46) then gives

$$\begin{aligned} E(D_0) &= \frac{6}{p\pi\theta} \left( \frac{\alpha}{\alpha_0} \right)^{0.9} \int_0^{\omega_{\text{max}}} \left[ 1 \right. \\ &\quad \left. - \frac{2}{\pi\theta} \left( \frac{\alpha}{\alpha_0} \right)^{0.9} \ln(\sec\omega + \tan\omega) \right]^{3/p-1} d\omega \end{aligned} \quad (57)$$

where  $\omega_{\text{max}}$  is the value of  $\omega$  for which  $\zeta=1$ ; specifically,

$$\omega_{\text{max}} = \tan^{-1} \left[ \frac{1}{2} \left( q - \frac{1}{q} \right) \right] \quad (58)$$

Table 1 Combustion efficiencies  $E$  for the two-dimensional zero-lag models<sup>a</sup>

$\theta$	Exact, Eqs. (53), (54), (49)			Delta-function approximation, Eqs. (46) and (47)	Constant- $\alpha$ approximation, Eq. (57)
	$\langle\theta\rangle=0.1$	$\langle\theta\rangle=1.0$	$\langle\theta\rangle=10.0$		
0.1	0.997	0.998	0.998	0.997	0.997
0.2	0.987	0.991	0.992	0.987	0.987
0.5	0.912	0.947	0.953	0.930	0.930
1.0	0.738	0.822	0.848	0.801	0.793
2.0	0.489	0.587	0.639	0.590	0.565
5.0	0.229	0.288	0.332	0.315	0.280
10.0	0.120	0.153	0.180	0.176	0.150
20.0	0.0615	0.0788	0.0932	0.0937	0.0771
50.0	0.0249	0.0320	0.0381	0.0390	0.0314

<sup>a</sup> $p=3/2$ ,  $\phi=0.45$ ,  $\sigma=0.46$ .

where

$$q = \exp \left[ \frac{\pi \theta}{2} \left( \frac{\alpha_0}{\alpha} \right)^{0.9} \right] \quad (59)$$

All that remains is to choose a suitable value for  $\alpha$ . The most obvious unbiased choice is the average of the values corresponding to the propellant surface (before any oxidizer has been consumed) and to complete combustion of the aluminum. For a delta function  $F(D_0)$ , at least, this gives

$$\frac{\alpha}{\alpha_0} = \frac{1}{2} [1 + (1 - \phi)] = 1 - \frac{\phi}{2} \quad (60)$$

and this value will be used in all numerical work.

#### Numerical Comparison of the Zero-Lag Models

With regard to the dependence of aluminum combustion efficiency on initial particle size, there are two ways in which the models of the preceding sections can be compared. First, one can observe the variation in  $E$  with  $\theta$  for a given value of  $\langle \theta \rangle$  (and fixed values of  $p$ ,  $\beta$ , and  $\phi$ ). [As is evident from Eq. (49), the form of the function  $E(\theta)$  is influenced by the value of  $\langle \theta \rangle$  simply because the depletion of oxidizer in the vicinity of a given particle is affected by the average size of all neighboring particles.] Secondly, one can examine the variation in  $\bar{E}$  with  $\langle \theta \rangle$ . Although only the latter has any immediate implications for rocket performance, the former is also of interest because most of the existing results are presented in a similar format.

Before either set of computations can be carried out, of course, the form of the function  $F(D_0)$  must be specified. According to both Hermesen<sup>2</sup> and King,<sup>3</sup> a reasonable choice (in the absence of detailed information) is the log-normal distribution

$$F(D_0) = \frac{1}{\sigma \sqrt{2\pi} D_0} \exp \left[ -\frac{1}{2} \left( \frac{1}{\sigma} \ln \frac{D_0}{D_m} \right)^2 \right] \quad (61)$$

with a standard deviation of  $\sigma = 0.46$  and an adjustable "mean" value  $D_m$ . From this it can be shown that, for any  $j$

$$\langle D_0^j \rangle = D_m^j e^{j^2 \sigma^2 / 2} \quad (62)$$

and thus

$$\beta = e^{-9\sigma^2/4} \quad (63)$$

which provides the numerical value  $\beta = 0.621$ . Now, in terms of the new variable

$$\eta = \frac{1}{\sqrt{2}} \left( \frac{1}{\sigma} \ln \frac{D_0}{D_m} - 3\sigma \right) \quad (64)$$

Eq. (10), when combined with Eq. (61), can be rewritten in the simple form

$$\bar{E} = \frac{1}{\sqrt{\pi}} \int_{-\infty}^{\infty} e^{-\eta^2} E(\eta) d\eta \quad (65)$$

Any of the models discussed above can be used to evaluate  $E(\eta)$ ; however, since  $E$  is generally computed for a given value of  $\theta$ , rather than  $\eta$ , a relation between the two quantities is needed. This can be determined (for the case  $p = 3/2$ ) from Eqs. (22), (62), and (64):

$$\theta = \langle \theta \rangle \exp \left[ \frac{3\sigma}{2} \left( \eta \sqrt{2} + \frac{9\sigma}{4} \right) \right] \quad (66)$$

Finally, it should be noted that the last term in Eq. (49) becomes, on substitution of Eq. (61),

$$\frac{4\phi\beta}{3\sigma(2\pi)^{1/2}} \left( \frac{\theta}{\langle \theta \rangle} \right)^2 \exp \left[ -2 \left( \frac{1}{3\sigma} \ln \frac{\theta}{\beta^{1/2} \langle \theta \rangle} \right)^2 \right] \zeta^{-1} \left( \frac{d\zeta}{da} \right)^4$$

so that neither  $D_0$  nor  $D_m$  appears explicitly.

Considering first the function  $E(\theta)$ , Table 1 compares the "exact" predictions of Eqs. (53), (54), and (49) [for three different choices of  $\langle \theta \rangle$ ] with the values computed from Eqs. (46) and (47), based on a monodisperse agglomerate population, and Eq. (57), based on a constant oxidizer concentration. For consistency,  $p$  is set equal to 3/2 throughout; the value adopted for  $\phi$ , 0.45, is appropriate to a propellant with a hydrocarbon binder.<sup>5</sup> (More modern propellants tend to give somewhat larger equivalence ratios, provided that the gas composition is calculated at the bulk chamber temperature.) It should be mentioned that the use of Eqs. (46) and (47) in this comparison is, strictly speaking, invalid; since these equations were derived for a delta function  $F(D_0)$ , each entry in this column of the table actually corresponds to a different value of  $\langle \theta \rangle$ . Ignoring this, however, can be regarded simply as an approximation—one that assumes that particles of different sizes act independently insofar as their effects on the depletion of oxidizer are concerned. This is essentially the approach that is taken by King.<sup>3</sup> It remains to be seen whether this approximation is better or worse than that underlying Eq. (57).

Table 2 Overall combustion efficiencies  $\bar{E}$  for the zero-lag models<sup>a</sup>

$\langle \theta \rangle$	One-dimensional approximation, Eqs. (65), (27)	Exact Eqs. (65), (53), (54), (49)	Delta-function approximation, Eqs. (65), (46), (47)	Constant- $\alpha$ approximation, Eqs. (65), (57)
0.02	0.972	0.998	0.999	0.999
0.05	0.935	0.990	0.992	0.992
0.1	0.882	0.967	0.972	0.972
0.2	0.801	0.910	0.920	0.917
0.5	0.643	0.752	0.762	0.750
1.0	0.498	0.578	0.581	0.558
2.0	0.351	0.394	0.392	0.363
5.0	0.189	0.202	0.200	0.175
10.0	0.108	0.112	0.110	0.0929
20.0	0.0577	0.0588	0.0583	0.0479
50.0	0.0241	0.0243	0.0242	0.0195

<sup>a</sup>  $p = 3/2$ ,  $\phi = 0.45$ ,  $\sigma = 0.46$ .

The table shows that the results provided by the two approximate methods do not agree particularly well with the more rigorous values over the entire range of  $\theta$ , especially for small values of  $\langle\theta\rangle$ . However, this will not necessarily have any serious practical consequences: the discrepancy is large only for values of  $\theta$  that differ substantially from the prevailing  $\langle\theta\rangle$ —the delta-function results are somewhat better in this regard—and such values will have little influence on  $\bar{E}$  if the distribution function  $F(D_0)$  is reasonably narrow.

A more significant test of the formulas, then, is a comparison of the predictions of  $\bar{E}$  vs  $\langle\theta\rangle$ . Table 2 contains the numerical results for this case, with  $E(\eta)$  being calculated via Eqs. (27); (53), (54), and (49); (46) and (47); and (57). All fixed parameters are assigned the same values as in Table 1. Clearly, the delta-function approximation gives excellent results over the entire range of  $\langle\theta\rangle$ . The values predicted by the one-dimensional analysis are in general only fair, and good accuracy is attained only for small  $\bar{E}$  (which is not a situation of great practical importance). As noted earlier by King,<sup>3</sup> the combustion efficiency is underpredicted for all  $\langle\theta\rangle$ . The constant- $\alpha$  approach is entirely adequate when  $\bar{E}$  is near unity, but it fails somewhat at smaller values. This is not surprising; when  $\bar{E}$  is small, most of the aluminum particles do not burn completely in the chamber, and the average value of  $\alpha$  given by Eq. (60) is not likely to be satisfactory.

The success of the delta-function approximation is both gratifying and of considerable practical importance. First, it means that the function  $E(\theta)$  can be computed once and for all, without regard to the nature of  $F(D_0)$  (just as for the constant- $\alpha$  case), rather than having to be reevaluated for each new situation. Furthermore, the computation itself becomes a great deal simpler. While there is only a modest savings of effort in the zero-lag model considered above, the simplification is enormous when velocity lags are included (which is often necessary for truly accurate results). Consequently, the approximation will be used to full advantage in the following section.

#### Two-Dimensional Flowfield with Particle Velocity Lags Included

When particle velocity lags are not negligible, a distinction must be made between the velocity components of the gas,  $U$  and  $V$ , and those of the particle phase,  $u$  and  $v$ . The former are given by Eqs. (28) and (29), but the latter must be found by solving the particle equations of motion. Provided that interparticle interactions and lift forces<sup>11</sup> can be ignored, each equation of motion takes the form of an equality between the convective acceleration and the viscous drag. Thus

$$u \frac{\partial u}{\partial x} + v \frac{\partial u}{\partial r} = \frac{18\mu\lambda}{\rho_{Al}D^2} (U - u) \quad (67)$$

$$u \frac{\partial v}{\partial x} + v \frac{\partial v}{\partial r} = \frac{18\mu\lambda}{\rho_{Al}D^2} (V - v) \quad (68)$$

where  $\mu$  is the gas viscosity and  $\lambda$  is the ratio of the actual drag force to that given by Stokes' law. A standard correlation for  $\lambda$  is<sup>12</sup>

$$\lambda = 1 + 0.15Re_l^{0.687} \quad (69)$$

where  $Re_l$  is the local Reynolds number,

$$Re_l = \frac{D\rho_g}{\mu} [(U - u)^2 + (V - v)^2]^{1/2} \quad (70)$$

$\rho_g$  being the gas density. Now, clearly, Eqs. (67) and (68) must be solved in conjunction with an equation for the parti-

cle diameter, and this can be obtained from Eq. (4):

$$u \frac{\partial D}{\partial x} + v \frac{\partial D}{\partial r} = -kD^{1-p}\alpha^{0.9} \quad (71)$$

This, in turn, necessitates an equation for  $\alpha$ , which can be derived in a like manner from Eq. (37), noting, of course, that the appropriate velocity components here are  $U$  and  $V$ . For the special case in which  $F(D_0)$  is a delta function, one has

$$U \frac{\partial \alpha}{\partial x} + V \frac{\partial \alpha}{\partial r} = -\frac{3\pi k \rho_{Al}}{4M_{Al}c} n \alpha^{0.9} D^{3-p} \quad (72)$$

However, the particle number density  $n$  is no longer a constant, because  $\nabla \cdot \mathbf{u}$  is not equal to zero in the current situation. Thus,  $n$  must be determined by using the general conservation equation

$$u \frac{\partial n}{\partial x} + v \frac{\partial n}{\partial r} = -n \left( \frac{\partial u}{\partial x} + \frac{\partial v}{\partial r} + \frac{v}{r} \right) \quad (73)$$

(Implicit in this is the assumption that  $u$  and  $v$  are unique functions of  $x$  and  $r$ , which can be true only if  $F(D_0)$  is a delta function.) Equations (67), (68), and (71-73) now constitute a closed set of PDE's, for which the boundary conditions at  $r=R$  are  $u=v=0$  (each particle starts at rest),  $D=D_0$ ,  $\alpha=\alpha_0$ , and  $nv=-\dot{n}_0$ , from Eq. (34). It is apparent that the formulation of the problem—and, to an even greater degree, its solution—would be considerably more complicated for a general function  $F(D_0)$ .

Since the equations given above do not allow the tracing of individual particle trajectories, the method previously used to calculate the combustion efficiency cannot be applied (there is no way to relate a given  $D$  to a particular  $x_0$ ). An alternative, though, is to compute the quantity  $\dot{m}$  by integrating over the cross section of the chamber:

$$\dot{m} = \frac{\pi^2 \rho_{Al}}{3M_{Al}} \int_0^R u n D^3 r dr \quad (74)$$

so that

$$E = 1 - \frac{1}{R\dot{n}_0 D_0^3} \int_0^R u n D^3 r dr \quad (75)$$

In order to nondimensionalize the equations and to eliminate certain singularities (as well as the awkward boundary condition on  $n$ ), it is now convenient to introduce the new variables  $\hat{u} = uc/2\dot{r}_s N$ ,  $\hat{v} = vc/2\dot{r}_s N$ ,  $A = (D/D_0)^2$ ,  $\hat{\alpha} = \alpha/\alpha_0$ ,  $J = -nv/\dot{n}_0$ ,  $\hat{x} = x/R$ , and  $s = (1-r/R)^{1/2}$ . After the equations are rewritten, the caret notation can be dropped for simplicity; the new versions of Eqs. (67), (68), and (70) are then

$$\begin{aligned} A \left( u \frac{\partial u}{\partial x} - \frac{v}{2s} \frac{\partial u}{\partial s} \right) \\ = \frac{9}{\tau} \lambda \left\{ \frac{\pi}{2} x \sin[\pi(s^2 - \frac{1}{2}s^4)] - u \right\} \end{aligned} \quad (76)$$

$$\begin{aligned} A \left( u \frac{\partial v}{\partial x} - \frac{v}{2s} \frac{\partial v}{\partial s} \right) \\ = \frac{9}{\tau} \lambda \left\{ \frac{-1}{2(1-s^2)} \cos[\pi(s^2 - \frac{1}{2}s^4)] - v \right\} \end{aligned} \quad (77)$$

$$Re_l = 2ReA^{1/2} \left( \left\{ \frac{\pi}{2} x \sin[\pi(s^2 - 1/2s^4)] - u \right\}^2 + \left\{ \frac{1}{2(1-s^2)} \cos[\pi(s^2 - 1/2s^4)] + v \right\}^2 \right)^{1/2} \quad (78)$$

where

$$\tau = \frac{\rho_{Al} D_0^2 \dot{r}_s N}{\mu R c} \quad (79)$$

$$Re = \frac{D_0 \rho_g \dot{r}_s N}{\mu c} \quad (80)$$

Physically,  $\tau$  is the ratio of the characteristic velocity relaxation time to the mean residence time in the chamber and thus determines, to a large extent, the importance of the velocity lags;  $Re$  is the particle Reynolds number at the propellant surface. The remaining PDE's (71-73) become

$$u \frac{\partial A}{\partial x} - \frac{v}{2s} \frac{\partial A}{\partial s} = -\frac{2}{p\theta} A^{1-p/2} \alpha^{0.9} \quad (81)$$

$$\pi x \sin[\pi(s^2 - 1/2s^4)] v \frac{\partial \alpha}{\partial x} + \frac{1}{1-s^2} \times \cos[\pi(s^2 - 1/2s^4)] \frac{v}{2s} \frac{\partial \alpha}{\partial s} = \frac{3\phi}{p\theta} JA^{(3-p)/2} \alpha^{0.9} \quad (82)$$

$$u \frac{\partial J}{\partial x} - \frac{v}{2s} \frac{\partial J}{\partial s} = J \left( -\frac{\partial u}{\partial x} + \frac{u}{v} \frac{\partial v}{\partial x} - \frac{v}{1-s^2} \right) \quad (83)$$

The boundary conditions at  $s=0$  are simply that  $u=v=0$  and  $A=\alpha=J=1$ . Finally,  $E$  is now given by

$$E = 1 + \frac{2}{x} \int_0^1 \frac{u}{v} JA^{3/2} (1-s^2) s ds \quad (84)$$

It is important to note that  $E$  is no longer independent of the axial position  $x$  (or, therefore, of the chamber length); in fact,  $E$  is now a function of the six parameters  $p, \theta, \phi, \tau, Re$ , and  $x$ .

Once again, it is interesting to see how the analysis is altered for the case of constant  $\alpha$ . It would, of course, be possible simply to discard Eq. (82) and to solve the remaining equations in essentially the same manner as before, but it is much easier to formulate the problem in terms of particle trajectory equations:

$$\frac{dx}{dt} = u \quad (85)$$

$$\frac{dr}{dt} = v \quad (86)$$

$$\frac{du}{dt} = \frac{18\mu\lambda}{\rho_{Al} D^2} (U-u) \quad (87)$$

$$\frac{dv}{dt} = \frac{18\mu\lambda}{\rho_{Al} D^2} (V-v) \quad (88)$$

and Eq. (4). The corresponding initial conditions (at  $t=0$ , say) are that  $x=x_0$ ,  $r=R$ ,  $u=v=0$ , and  $D=D_0$ . Since  $\alpha$  is constant, Eq. (4) can be solved analytically:

$$D = (D_0^p - p k \alpha^{0.9} t)^{1/p} \quad (89)$$

The equations are now nondimensionalized by defining  $\hat{x}$ ,  $\hat{u}$ , and  $\hat{v}$  as before and introducing, in addition,  $\hat{r}=r/R$ ,  $\hat{D}=D/D_0$ , and  $\hat{t}=2\dot{r}_s N t/Rc$ ; the carets are then dropped. After this is done, Eqs. (85) and (86) are formally unchanged, while Eqs. (87-89) become

$$\frac{du}{dt} = \frac{9\lambda}{\tau D^2} \left[ \frac{\pi}{2} x \cos\left(\frac{\pi}{2} r^2\right) - u \right] \quad (90)$$

$$\frac{dv}{dt} = \frac{9\lambda}{\tau D^2} \left[ -\frac{1}{2r} \sin\left(\frac{\pi}{2} r^2\right) - v \right] \quad (91)$$

$$D = \left[ 1 - \left( \frac{\alpha}{\alpha_0} \right)^{0.9} \frac{t}{\theta} \right]^{1/p} \quad (92)$$

The initial conditions are that  $x=x_0$ ,  $r=1$ , and  $u=v=0$  at  $t=0$ . Once  $D$  has been evaluated at a given  $x$  for "all"  $x_0$  between 0 and  $x$ , the combustion efficiency can be computed in the usual fashion:

$$E = 1 - \frac{1}{x} \int_0^x D^3 dx_0 \quad (93)$$

Finally, it is instructive to carry out a set of calculations using King's pocket model,<sup>3</sup> according to which velocity lags are neglected in determining the oxidizer concentration along a particle trajectory. Mathematically, this amounts to using Eq. (40) in place of the constant- $\alpha$  assumption in the analysis of the preceding paragraph. It follows that Eq. (92) is replaced by

$$\frac{dD}{dt} = -\frac{1}{p\theta} D^{1-p} [1 + \phi(D^3 - 1)]^{0.9} \quad (94)$$

together with the condition that  $D=1$  at  $t=0$ . The computations are then performed in essentially the same manner as before.

It should be mentioned that the treatment of velocity lags in the above models is only an approximation, as it is based on a simplified picture of the true physical situation. Specifically, the analysis does not account for the fact that a small fraction (typically 5-15%<sup>13</sup>) of the condensed-phase  $Al_2O_3$ , which forms as a result of the combustion process, tends to collect on the surface of the burning aluminum particle in the form of an oxide lobe. (The remainder gives rise to a dense cloud of oxide smoke.) While this is presumably taken into account implicitly in the empirical burning-rate equation, it is neglected in the expressions for the drag force on the particle. The error involved is unlikely to be important, however, because the oxide lobe will not constitute a significant portion of the total mass of the particle until the particle itself is very small and its velocity lag has vanished. In any event, a more rigorous treatment would require currently unavailable quantitative information on the  $Al_2O_3$  condensation process and effects of nonsphericity.

#### Numerical Comparison of the Finite-Lag Models

The calculations that must be carried out to obtain numerical results from the constant- $\alpha$  and pocket models are straightforward; however, the variable- $\alpha$  case is more difficult because standard numerical methods tend to be unstable when applied to this system of PDE's. This problem is overcome by discretizing the equations in  $x$  and using a fully implicit packaged code<sup>14</sup> to solve the resulting system of ODE's.

Obviously, since  $E$  depends on so many parameters, a comprehensive numerical study is impractical, but it is also



**Table 3 Combustion efficiencies  $E$  for the two-dimensional finite-lag models<sup>a</sup>**

$\theta$	Variable $\alpha$	Constant $\alpha$	Pocket model
0.1	1.000	1.000	1.000
0.2	0.996	0.997	0.996
0.5	0.963	0.964	0.963
1.0	0.857	0.856	0.858
2.0	0.654	0.636	0.656
5.0	0.362	0.328	0.365
10.0	0.206	0.178	0.208
20.0	0.111	0.0927	0.112
50.0	0.0469	0.0380	0.0468

<sup>a</sup> $p=3/2$ ,  $\phi=0.45$ ,  $\tau=1.0$ ,  $Re=5.0$ ,  $x=5.0$ .

unnecessary for present purposes. Thus, as before,  $E$  will be tabulated vs  $\theta$  for a typical set of values of the other parameters:  $p=3/2$ ,  $\phi=0.45$ ,  $\tau=1.0$ ,  $Re=5.0$ ,  $x=5.0$ .

The results are presented in Table 3. As in the zero-lag case, the use of the constant- $\alpha$  approximation leads to significant errors when  $\theta$  is large, primarily because of the inadequacy of Eq. (60): if most of the particles do not burn completely, then the average value of  $\alpha$  suggested by the equation will be too small, and the combustion efficiency will consequently be underestimated. On the other hand, the pocket model gives highly accurate results for all  $\theta$ . A comparison of Tables 1 and 3 also shows that velocity lags lead to an increase in  $E$ . This is expected physically, of course, because such lags cause the particles to remain in the chamber for longer periods of time.

### Conclusion

A rigorous calculation of aluminum combustion efficiency, which accounts simultaneously for particle velocity lags, an arbitrary initial particle size distribution, and a varying oxidizer concentration, is a formidable task—so much so, in fact, that it has never been attempted. However, the work presented here indicates that it is usually not necessary to solve the problem in complete generality, for satisfactory results can be obtained in most cases by making a suitable approximation. First of all, if conditions are such that the velocity lags can be neglected, then the problem becomes much more manageable; in particular, a semianalytical solution is possible when the burning-time exponent has the (physically realistic) value  $3/2$ . Further simplification can be achieved via the so-called delta-function approximation, which asserts that the way in which oxidizer is depleted along a particle trajectory can be determined independently for particles of different initial sizes. While this is physically unrealistic, it can be expected to provide accurate values of the overall combustion efficiency  $\bar{E}$  if the actual size distribution is reasonably narrow. Numerical calculations using a typical value for the standard deviation  $\sigma$  show that excellent results can indeed be obtained in practical cases. In addition to simplifying the computation of a set of individual combustion efficiencies  $E(D_0)$ , the delta-function approximation has the enormous advantage that these values need not be recalculated for each new size distribution. The same savings of effort can be achieved by making the assumption that the oxidizer concentration  $\alpha$  is constant, as is done in the SPP computer code. However, the numerical results obtained here indicate that this approach leads to significant errors at low combustion efficiencies if an average value of  $\alpha$  is used. This situation could possibly be remedied somewhat by artificially adjusting  $\alpha$ , but this would require foreknowledge of the approximate value of  $E$  for any given set of conditions.

When particle velocity lags cannot be neglected, the computation of combustion efficiencies is cumbersome, even when the delta-function approximation is used. However,

the calculations can again be simplified, without any real sacrifice of accuracy, by making the additional assumption that the lags do not significantly affect the oxidizer concentration profile along a particle trajectory.

In essence, then, the work presented here can be viewed as a justification for the so-called pocket model used by King.<sup>3</sup> As noted earlier, this model actually involves two major assumptions, namely, that particles of different sizes act independently insofar as oxidizer depletion is concerned and that this depletion is unaffected by velocity lags. By necessity, these assumptions are examined separately rather than simultaneously in the foregoing analysis; nevertheless, the results strongly suggest that the pocket model is an adequate approximation in most cases.

### Appendix

The first step in converting Eq. (48) to a pure differential equation is to multiply through by  $F(D_0)$  and then integrate over  $D_0$  from  $D_0^*(\alpha)$  to infinity. With the aid of Leibniz' rule for differentiating an integral, this gives

$$\begin{aligned} \frac{d}{d\alpha} \int_{D_0^*(\alpha)}^{\infty} D^{3/2} F(D_0) dD_0 \\ = \frac{2M_{Al}c}{\pi n \rho_{Al}} \left[ \int_{D_0^*(\alpha)}^{\infty} D^{3/2} F(D_0) dD_0 \right]^{-1} \int_{D_0^*(\alpha)}^{\infty} F(D_0) dD_0 \end{aligned} \quad (A1)$$

Separating variables and integrating, one finds

$$\begin{aligned} \int_{D_0^*(\alpha)}^{\infty} D^{3/2} F(D_0) dD_0 \\ = \left[ \langle D_0^{3/2} \rangle^2 + \frac{4M_{Al}c}{\pi n \rho_{Al}} \int_{\alpha_0}^{\alpha} \int_{D_0^*(\psi)}^{\infty} F(D_0) dD_0 d\psi \right]^{1/2} \end{aligned} \quad (A2)$$

This is now back-substituted into Eq. (48), which can then be integrated to yield

$$\begin{aligned} D^{3/2} - D_0^{3/2} = \frac{2M_{Al}c}{\pi n \rho_{Al}} \int_{\alpha_0}^{\alpha} \left[ \langle D_0^{3/2} \rangle^2 \right. \\ \left. + \frac{4M_{Al}c}{\pi n \rho_{Al}} \int_{\alpha_0}^{\psi} \int_{D_0^*(\psi')}^{\infty} F(\nu) d\nu d\psi' \right]^{-1/2} d\psi \end{aligned} \quad (A3)$$

By definition,  $D_0$  is equal to  $D_0^*$  when  $D=0$  for a given  $\alpha$ . Making these replacements in Eq. (A3), one sees that the quantities  $D_0^{3/2} - D^{3/2}$  and  $D_0^{*3/2}$  are identical functions of  $\alpha$ . This fact can then be used to eliminate  $D_0^*$  from the right-hand side of the equation. Thus, in terms of the dimensionless variables  $\zeta = 1 - (D/D_0)^{3/2}$  and  $a = 1 - \alpha/\alpha_0$ , one has

$$\zeta = \frac{\langle \theta \rangle}{2\phi\beta\theta} \int_0^a \left[ 1 - \frac{1}{\phi\beta} \int_0^{\psi'} \int_{D_0^{\zeta^{2/3}(\psi')}}^{\infty} F(\nu) d\nu d\psi' \right]^{-1/2} d\psi' \quad (A4)$$

where  $\beta$  is defined in Eq. (50). The desired result can now be obtained by differentiating three times with respect to  $a$ :

$$\frac{d\zeta}{da} = \frac{\langle \theta \rangle}{2\phi\beta\theta} \left[ 1 - \frac{1}{\phi\beta} \int_0^a \int_{D_0^{\zeta^{2/3}(\psi')}}^{\infty} F(\nu) d\nu d\psi' \right]^{-1/2} \quad (A5)$$

$$\frac{d^2\zeta}{da^2} = 2\phi\beta \left( \frac{\theta}{\langle \theta \rangle} \right)^2 \left( \frac{d\zeta}{da} \right)^3 \int_{D_0^{\zeta^{2/3}(a)}}^{\infty} F(\nu) d\nu \quad (A6)$$

and Eq. (49). The initial conditions for use with Eq. (49) follow directly from Eqs. (A4–A6).

## References

- <sup>1</sup>Price, E. W., "Combustion of Metalized Propellants," *Progress in Astronautics and Aeronautics: Fundamentals of Solid-Propellant Combustion*, Vol. 90, AIAA, New York, 1984, pp. 479-513.
- <sup>2</sup>Hermesen, R. W., "Aluminum Combustion Efficiency in Solid Rocket Motors," AIAA Paper 81-0038, Jan. 1981.
- <sup>3</sup>King, M. K., "Prediction of Metal Combustion Efficiency in Low Port-to-Throat Area Ratio and Nozzleless Solid Rocket Motors," AIAA Paper 82-1202, June 1982.
- <sup>4</sup>King, M. K., "Metal Combustion Efficiency Predictions for Low  $L^*$  Rocket Motors," *Journal of Spacecraft and Rockets*, Vol. 22, Sept. 1985, pp. 512-513.
- <sup>5</sup>Siegel, B. and Schieler, L., *Energetics of Propellant Chemistry*, Wiley, New York, 1964, pp. 149-151.
- <sup>6</sup>Pokhil, P. F., Belyayev, A. F., Frolov, Y. V., Logachev, V. S., and Korotkov, A. I., "Combustion of Powdered Metals in Active Media," Foreign Technology Division, Wright-Patterson Air Force Base, OH, FTD-MT-24-551-73, Oct. 1973, pp. 198-200.
- <sup>7</sup>Davis, A., "Solid Propellants: The Combustion of Particles of Metal Ingredients," *Combustion and Flame*, Vol. 7, Dec. 1963, pp. 359-367.
- <sup>8</sup>King, M. K., "Modeling of Single Particle Aluminum Combustion," Air Force Office of Scientific Research, Bolling Air Force Base, Washington, DC, AFOSR-TR-78-0060, Nov. 1977, pp. 75-130.
- <sup>9</sup>Culick, F. E. C., "Rotational Axisymmetric Mean Flow and Damping of Acoustic Waves in a Solid Propellant Rocket," *AIAA Journal*, Vol. 4, Aug. 1966, pp. 1462-1464.
- <sup>10</sup>Dunlap, R., Willoughby, P. G., and Hermesen, R. W., "Flowfield in the Combustion Chamber of a Solid Propellant Rocket Motor," *AIAA Journal*, Vol. 12, Oct. 1974, pp. 1440-1442.
- <sup>11</sup>Ishii, R., "Motion of Small Particles in a Gas Flow," *Physics of Fluids*, Vol. 27, Jan. 1984, pp. 33-41.
- <sup>12</sup>Torobin, L. B. and Gauvin, W. H., "Fundamental Aspects of Solids-Gas Flow, Part I: Introductory Concepts and Idealized Sphere Motion in Viscous Regime," *Canadian Journal of Chemical Engineering*, Vol. 37, Aug. 1959, pp. 129-141.
- <sup>13</sup>Price, E. W., Sigman, R. K., Sambamurthi, J. K., and Park, C. J., "Behavior of Aluminum in Solid Propellant Combustion," Air Force Office of Scientific Research, Bolling Air Force Base, Washington, DC, AFOSR F 49620-78-C-0003/49620-82-C-0013, June 1982, p. 39.
- <sup>14</sup>Petzold, L. R., "A Description of DASSL: A Differential-Algebraic System Solver," Sandia National Laboratories, Livermore, CA, SAND82-8637, Sept. 1982.

*From the AIAA Progress in Astronautics and Aeronautics Series...*

## COMBUSTION DIAGNOSTICS BY NONINTRUSIVE METHODS – v. 92

*Edited by T.D. McCay, NASA Marshall Space Flight Center  
and  
J.A. Roux, The University of Mississippi*

This recent Progress Series volume, treating combustion diagnostics by nonintrusive spectroscopic methods, focuses on current research and techniques finding broad acceptance as standard tools within the combustion and thermophysics research communities. This book gives a solid exposition of the state-of-the-art of two basic techniques—coherent antistokes Raman scattering (CARS) and laser-induced fluorescence (LIF)—and illustrates diagnostic capabilities in two application areas, particle and combustion diagnostics—the goals being to correctly diagnose gas and particle properties in the flowfields of interest. The need to develop nonintrusive techniques is apparent for all flow regimes, but it becomes of particular concern for the subsonic combustion flows so often of interest in thermophysics research. The volume contains scientific descriptions of the methods for making such measurements, primarily of gas temperature and pressure and particle size.

*Published in 1984, 347 pp., 6 × 9, illus., \$39.50 Mem., \$69.50 List; ISBN 0-915928-86-8*

**TO ORDER WRITE: Publications Order Dept., AIAA, 1633 Broadway, New York, N.Y. 10019**